TransNav
http://www.transnav.eu
the International Journal on Marine Navigation and Safety of Sea Transportation
Volume 18
Number 2
June 2024

DOI: 10.12716/1001.18.02.22

Numerical Prediction of Ship's Self-Propulsion Parameter by Using CFD Method

N.T.N. Hoa
Ho Chi Minh City University of Transport, Ho Chi Minh, Vietnam

ABSTRACT: This paper reports the results of numerical simulations of ship self-propulsion using the computational fluid dynamics (CFD) method. The sliding mesh method is utilized to model the actual propeller working behind the ship. In addition, the volume of fluid method was applied to accurately track and solve the free surface. Some several important factors such as mesh generation, time step, turbulence model that can affect the accuracy of the obtained simulation results are discussed in this research. The Benchmark Japanese Bulk Carrier vessel was used in this study as the case study. The numerical obtained results are compared with measured data to verify and validate the numerical results.

1 INTRODUCTION

The prediction of a ship's self-propulsion parameters is a challenging task in ship hydrodynamics in general and in the ship power estimation in particular due to the accuracy in evaluating this parameter will effect on accurate power estimation.

Among various methods to evaluate the ship's self-propulsion, the CFD method is the most commonly used due to its accuracy and computational time [1-4]. Therefore, this paper aims to evaluate the ship's self-propulsion based on the CFD method.

Nowadays, according to CFD method, there are two different approaches for predicting ship's self-propulsion point, which consists of using the actual propeller and using virtual disk instead of the actual propeller, some previous research works using these approaches are reported in the literatures [3-19]. Although, the advantage of virtual disk method is simple and faster in predicting the ship's self-propulsion, it is unable to provide detailed information about flow around the propeller. However, using actual propeller method can provide us all the information about flow field in the wake regions efficiently and reliably. Therefore, this study used actual propeller method to evaluate the ship's self-propulsion parameters.

Previous research has employed the actual propeller method to evaluate the self-propulsion characteristics of a ship. Tu T.N. et al [3] utilized the CFD method to investigate the interaction between the hull of the ship and propeller, as well as the propulsive coefficients for the actual propeller. The simulation results showed good agreement with measured data. Castro, A.M., et al. [10] used actual propeller method to evaluate the ship's self-propulsion parameters for containership at full-scale. The obtained simulation results are agreed well with the available data. In the research of Sun, W., et al. [20] actual propeller method was used to performed self-propulsion simulation. The numerical results obtained for ship self-propulsion in full-scale shows good agreement with the measured data. The previous studies have played a vital role in predicting propulsive coefficients, and this study uses the actual propeller method to simulate the self-propulsion of the JBC ship in model-scale. The sliding mesh method was applied to model actual propeller located behind the ship.

2 MATERIAL AND METHOD

2.1 *Flow model*

The Reynolds-Averaged Navier-Stokes Equations (RANSE) is amended with the force *Fv*. This represents the propeller acting on the fluid as given in Equation 1.

$$\overline{u}_j \frac{\partial \overline{u}_i}{\partial x_j} = \frac{1}{\rho}\left(\mu \frac{\partial^2 \overline{u}_i}{\partial x_j^2} - \frac{\partial \tau_{ij}}{\partial x_i} - \frac{\partial \overline{p}}{\partial x_i} + F_v \right) \tag{1}$$

where ρ is the fluid densit, μ is the dynamic viscosity, τ_{ij} is the Reynolds stress, p presents the mean pressure, $\overline{u}_i$ presents the averaged Cartesian components.

The RANSE are defined as follows:

$$\frac{\partial(\rho \overline{u}_i)}{\partial x_i} = 0 \tag{2}$$

$$\frac{\partial(\rho \overline{u}_i)}{\partial t} + \frac{\partial}{\partial x_j}\left(\rho \overline{u}_i \overline{u}_j + \rho \overline{u_i' u_j'} \right) = -\frac{\partial \overline{p}}{\partial x_i} + \frac{\partial \overline{\tau}_{ij}}{\partial x_j} \tag{3}$$

where x_i and $\overline{u}_i$ are the position and velocity vector, ρ is the fluid density, $\rho \overline{u_i' u_j'}$ is the Reynolds stress tensor, $\overline{p}$ is the mean pressure, t is the time and $\overline{\tau}_{ij}$ is the mean viscous stress tensor.

$\overline{\tau}_{ij}$ is defined as follows:

$$\overline{\tau}_{ij} = \mu\left(\frac{\partial \overline{u}_i}{\partial x_j} + \frac{\partial \overline{u}_j}{\partial x_i} \right) \tag{4}$$

where μ is the dynamic viscosity.

2.2 *Turbulence model*

The Realizable k- ε two-layer model is one of the turbulence models that calculates the eddy viscosity by solving equations for k and ε. This model is designed to accurately predict the turbulent flow in a wide range of applications.

$$\mu_t = \rho C_\mu f_\mu k T \tag{4}$$

where f_μ is a damping function, T is a turbulent time scale and C_μ is a model coefficient.

Eqn. (6) determines the turbulent time scale as follow:

$$T = T_e \tag{6}$$

The transport equations for k and the ε are given as follows:

$$\frac{\partial}{\partial t}(\rho k) + \nabla \cdot (\rho k \overline{\mathrm{v}}) = \nabla \cdot \left[\left(\mu + \frac{\mu_t}{\sigma_k} \right) \nabla k \right] + P_k - \rho(\varepsilon - \varepsilon_0) + S_k \tag{7}$$

$$\begin{aligned} \frac{\partial}{\partial t}(\rho \varepsilon) + \nabla \cdot (\rho \varepsilon \overline{\mathrm{v}}) = \nabla \cdot \left[\left(\mu + \frac{\mu_t}{\sigma_\varepsilon} \right) \nabla \varepsilon \right] + \frac{1}{T_e} C_{\varepsilon 1} P_\varepsilon - \\ C_{\varepsilon 2} f_{2\rho} \left(\frac{\varepsilon}{T_e} - \frac{\varepsilon_0}{T_0} \right) + S_\varepsilon \end{aligned} \tag{8}$$

Production terms P_k and P_ε are given by Eqn. (9) as follow:

$$P_k = f_c G_k + G_b - \gamma_M ; \; P_\varepsilon = f_c S k + C_{\varepsilon 3} G_b \tag{9}$$

The damping functions is given by Eqn. (10) as follow:

$$\begin{aligned} f_2 &= \frac{k}{k + \sqrt{\upsilon \varepsilon}} ; \\ f_\mu &= \frac{1}{C_\mu \left\{ 4 + \sqrt{6} \cos\left[\frac{1}{3} \cos^{-1}\left(\sqrt{6} \frac{S^{*3}}{\sqrt{S^* : S^{*3}}} \right) \right] \right\} \frac{k}{\varepsilon} \sqrt{S:S + W:W}} \end{aligned} \tag{10}$$

3 NUMERICAL SIMULATION

3.1 *Case study*

The vessel used as a case study in this study is JBC vessel. This vessel was developed by the Japanese National Maritime Research Institute. The simulation is conducted at a model-scale of λ=40, so it allows us to carry out a direct comparison with experimental data. The hull form and propeller specifications of the JBC vessel are listed in Tables 1 and 2. For further visualization, Figures 1 and 2 provide views of the ship and its propeller. The towing tank measured data for JBC are available in [21, 22], providing a reliable source for comparison with the simulation results.

Table 1. JBC ship parameters

Descriptions		Unit	Value
Ship length	L	[m]	7.000
Ship breadth	B	[m]	1.1250
Design ship draft	T	[m]	0.4125
Volume displacement	∇	[m^3]	2.787
Froude number	Fr	[-]	0.1420

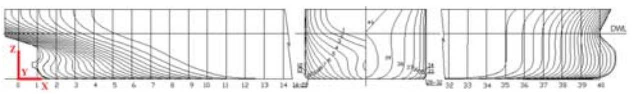

Figure 1. The geometry of JBC vessel

Table 2. Propeller parameters

Descriptions		Unit	Value
Diameter of propeller	D_P	[m]	0.203
Angle of rake	Θ	[deg.]	5
Expanded area ratio	AE/A0	[-]	0.500
Boss ratio	Dh/D_P	[-]	0.18
Pitch ratio	$P0.7/D_P$	[-]	0.750
Number of blades	Z	[-]	5
Direction of rotation	-	[-]	Clockwise

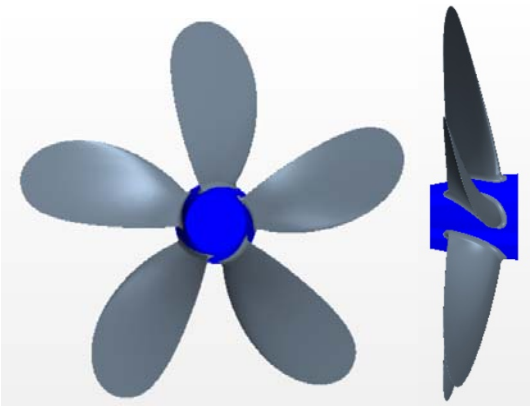

Figure 2. Views of JBC propeller

The simulation setup for this test case study replicates the towing tank test conditions detailed in [21, 22]. The ship was tested without a rudder at a design draft of 4125m and a Froude number of 0.1420. The ship's pitch and heave motions were kept free, and the environment condition was calm water.

3.2 *Numerical setup*

The simulation of ship's self-propulsion using the actual propeller method requires a computational domain that is divided into two zones: a stationary zone and a rotating sub-zone. The stationary zone encompasses the entire calculated domain and contains the ship hull, while the cylindrical rotating sub-zone contains the propeller. The stationary region is bounded by an inlet boundary located 1.5L to the ship bow, an outlet boundary located 2.5L behind the ship stern, and top and bottom boundaries located 1.5L and 2.5L from the ship. The side boundaries are positioned at 2.5L away from the ship in lateral direction. The size of the calculated domain conforms to the ITTC [3, 23]. A visual representation of the calculated domain is depicted in Figure 3.

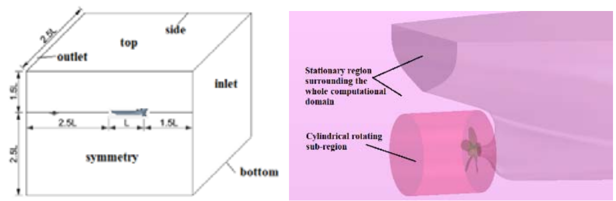

Figure 3. The calculated domain for self-propulsion prediction

The type of boundary condition was setup as follows [3, 4]: The top, inlet, and bottom boundaries are classified as velocity inlets, while the outlet is subject to pressure conditions. The side boundaries are set as symmetry planes. Additionally, the boundary conditions are set for the ship hull surface and propeller are no-slip wall.

Table-3 presents the physics model settings used in this study. The Volume of Fluid method was utilized for tracking and solving the free surface, and the Realizable k–ε turbulence model is chosen to close RANSE due to its proven accuracy in previous studies [24]. The vessel was permitted to move with heave and pitch motions. The propeller's rotation was introduced using the DFBI model, which enables the propeller to be attached to the ship's hull. An essential factor affecting the level of accuracy of the numerical results is the selection of the time-step size. To predict self-propulsion, a time-step size was chosen that results in the propeller rotating approximately 0.5 to 1.5 degrees per time step [23].

Table 3. Setup for physics model

Parameters	Setting
Solver	3D, implicit unsteady
Turbulence model	Realizable k–ε two layer
Multiphase model	The volume of fluid
Temporal discretization	First-order
Wall treatment	all wall y+ treatment

The numerical results are significantly affected by the mesh generation. In this research, a trimmed cell mesher was utilized to generate meshes for both stationary and cylindrical rotating sub-regions. The grid was refined at the free surface to accurately capture the Kelvin wave. Additionally, local volume grid refinements were implemented around the propeller, ship stern and ship bow regions, and the rotating sub-region to improve the resolution of the simulations. To accurately capture the interactions between the ship hull and the propeller, the trailing and leading edges of the propeller were subjected to additional refinement. Prism layers were also applied to resolve the boundary layer. The mesh consisted of a total of 8.7 million cells. Figure 4 displays the mesh generation results.

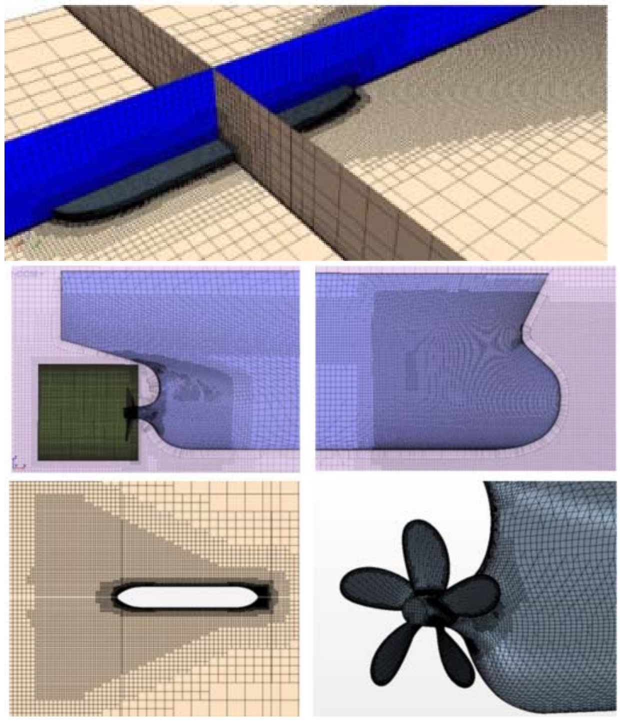

Figure 4. Some screenshots of the mesh system

4 RESULT AND DISCUSSION

In this study, the self-propulsion point was defined as the point at which the propeller thrust is equal to the resistance of the ship. However, in model scale simulations, it is necessary to take into account the Skin Friction Correction Force (SFC) that accounts for the variation in skin friction coefficients between the model scale and the full-scale ship. Ignoring this correction can lead to inaccurate results [25]

$$T = R_{T(SP)} - SFC \tag{11}$$

The SFC value used in this study was 18.2 N based on measured data [21, 22]. Since it is challenging to determine the self-propulsion in one run, so normally, two constant speed runs were carried out with two propeller revolution rates (n = 7.80 and n=8.00 rps). The linear interpolation method was used to determine the self-propulsion point. The time step was set at 3.5.10-4s.

The Table-4 in this study displays the results of the resistance and thrust as a function of the propeller's rotation rate. The self-propulsion point was identified at a rotation rate of 7.85 revolutions per second, as depicted in Figure 5. The comparison between the numerical results (CFD) and the measured data (EFD) is presented in Table 7. The results show a good agreement between the two datasets. The difference between the numerical results and the measured data was found to be 1.57%, 2.84% and 0.64% for resistance of the ship, thrust of propeller and self-propulsion point, respectively. Figure 6 presents a time history of resistance of the ship and propeller thrust at a rotation rate of 7.8 revolutions per second. The oscillations of propeller thrust are five times the rotational frequency due to the effect of ship hull form.

Table 4. Numerical obtained results

n [rps]	$R_{T(SP)}$ -SFC [N]	*T* [N]
7.80	22.85	22.55
8.00	23.85	24.75

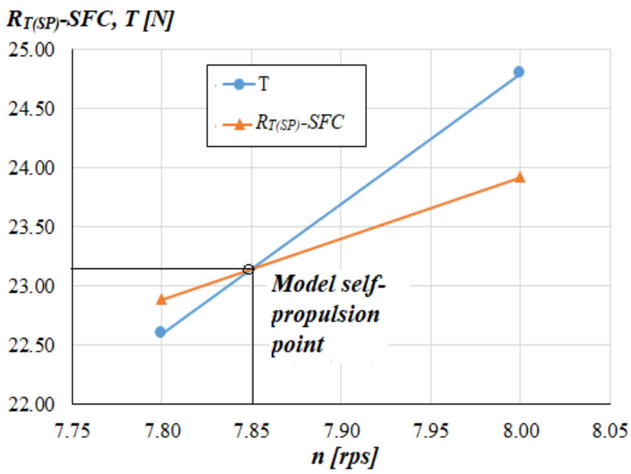

Figure 5. Defining the self-propulsion point procedure

Detailed flow characteristics around the ship hull and propeller in the self-propulsion simulation were also investigated. The figures illustrating these flow characteristics are presented in Figures from 7 to 12, respectively.

Table 5. Computed Self-propulsion point in comparison with measured data

Parameters		EFD [22]	CFD	E%D
RT(SP), [N]	$R_{T(SP)}$	40.760	41.39	1.57
T, [N]	*T*	22.560	23.19	2.84
Self-propulsion point	*n*	7.800	7.85	0.64

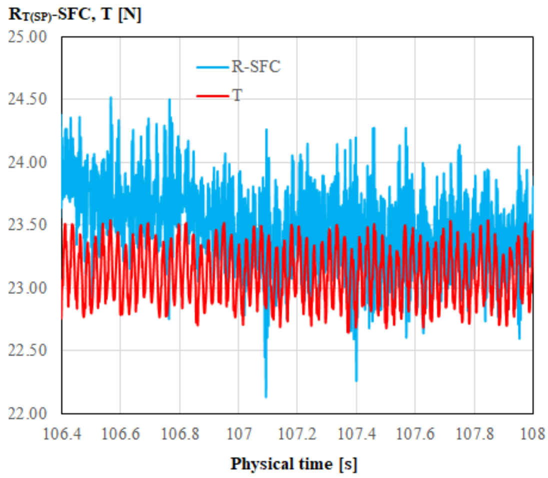

Figure 6. Time histories of resistance of the ship and thrust at *n*=7.8 rps.

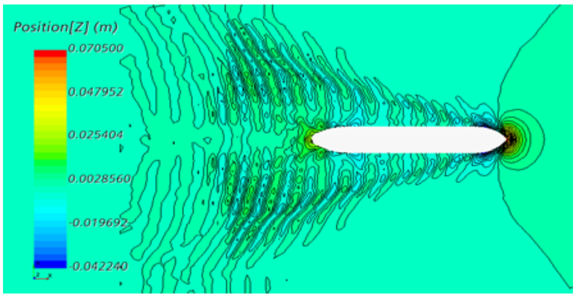

Figure 7. Wave-elevation at *n*=7.8 rps.

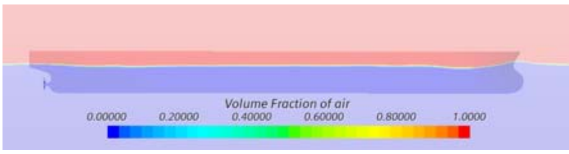

Figure 8. Water free surface at *n*=7.8 rps.

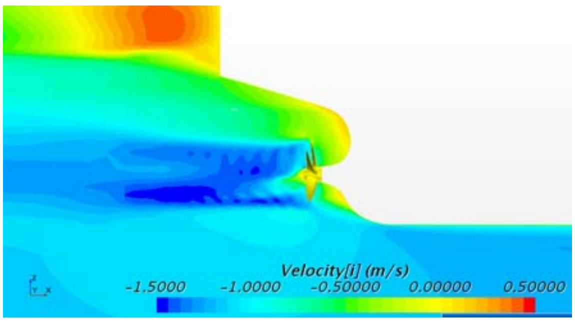

Figure 9. Velocity distribution in symmetry plane at *n*=7.8 rps.

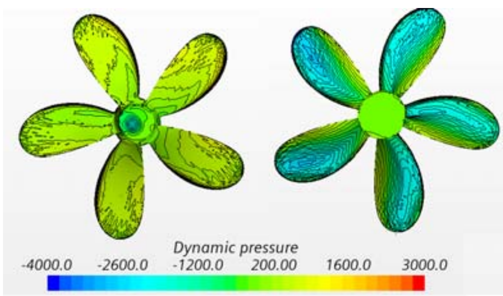

Figure-10. Dynamic pressure distribution on the blades surface of propeller at *n*=7.8 rps.

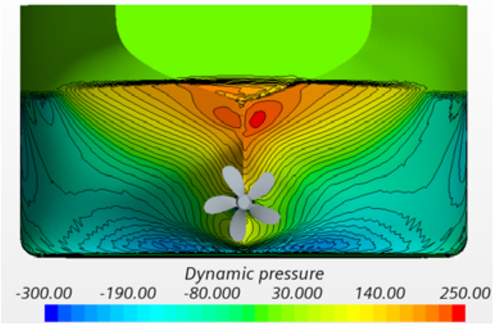

Figure 11. Dynamic pressure distribution on ship stern at n=7.8 rps.

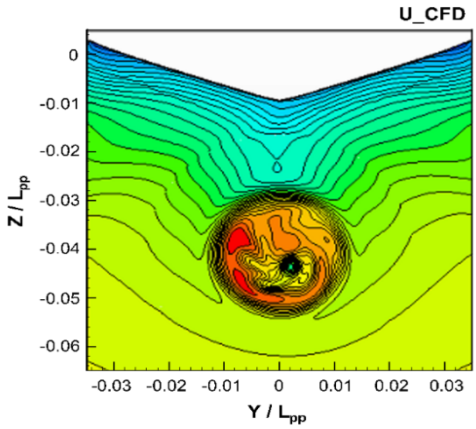

Figure 12. Comparion of velocity field in AP between CFD and EFD at n=7.8 rps.

The influence of propulsion models on the wake distribution at the aft perpendicular of the ship is depicted in Figure 11. It can be clearly observed in Figure 12, the wake can be classified into two zones, i.e. the zone inside the propeller and the zone outside the propeller. The first region showed an asymmetric form due to the propeller, while the other region is almost symmetric form.

Propeller working behind the ship will introduce pressure pulses on the ship hull above the propeller region, which may effect on noise and ship structure vibration. Figure 11 shows the influence of propeller on dynamic pressure distribution at the ship stern. As can be seen from Figure 13 the asymmetry in the dynamic pressure contours between the port and starboard side at the region of the hull above propeller.

5 CONCLUSIONS

The paper has successfully achieved its objectives. The study utilized the CFD method to evaluate the ship self-propulsion parameters. The sliding mesh method was applied to model the actual propeller located behind the ship. Ship is allowed to move with heave and pitch motion. Additionally, the paper dealt with various factors that impact the accuracy of simulation obtained results, such as choosing time step size, turbulence model and grid generation technique. The simulation results agreed well with the measured data, with differences between simulation and experimental results of 1.57%, 2.84% and 0.64% for resistance of the ship, thrust and self-propulsion point, respectively. Subsequent investigations will focus on enhancing the accuracy of the simulations by exploring various alternatives such as adjusting the grid generation process, increasing the mesh size, and using different turbulence models.

ACKNOWLEDGMENT

I acknowledge the support of time and facilities form Ho Chi Minh City University of Transport for this study.

REFERENCES

[1] Le, T.-H., et al., Numerical investigation on the effect of trim on ship resistance by RANSE method. Applied Ocean Research, 2021. 111: p. 102642.

[2] Choi, J., et al., Resistance and propulsion characteristics of various commercial ships based on CFD results. Ocean engineering, 2010. 37(7): p. 549-566.

[3] Tu, T.N., et al., Numerical prediction of propeller-hull interaction characteristics using RANS method. Polish Maritime Research, 2019.

[4] Gokce, M.K., O.K. Kinaci, and A.D. Alkan, Self-propulsion estimations for a bulk carrier. Ships Offshore Structures, 2019. 14(7): p. 656-663.

[5] Villa, D., S. Gaggero, and S. Brizzolara. Ship Self Propulsion with different CFD methods: from actuator disk to viscous inviscid unsteady coupled solvers. in The10th International Conference on Hydrodynamics. 2012.

[6] Song, K., et al., Simulation strategy of the full-scale ship resistance and propulsion performance. 2021. 15(1): p. 1321-1342.

[7] Soares, C.G. and T.A. Santos, Progress in Maritime Technology and Engineering: Proceedings of the 4th International Conference on Maritime Technology and Engineering (MARTECH 2018), May 7-9, 2018, Lisbon, Portugal. 2018: CRC Press.

[8] Jasak, H., et al., CFD validation and grid sensitivity studies of full scale ship self propulsion. International Journal of Naval Architecture and Ocean Engineering, 2019. 11(1): p. 33-43.

[9] Hu, J.-m., et al., Prediction of ship power and speed performance based on RANS method. 2017. 64(1-2): p. 51-78.

[10] Castro, A.M., et al., Full scale self-propulsion computations using discretized propeller for the KRISO container ship KCS. 2011. 51(1): p. 35-47.

[11] Carrica, P.M., A.M. Castro, and F. Stern, Self-propulsion computations using a speed controller and a discretized propeller with dynamic overset grids. Journal of marine science and technology, 2010. 15(4): p. 316-330.

[12] Chuan, T.Q., et al. Full-Scale Self-propulsion Computations Using Body Force Propeller Method for Series Cargo Ship 12500DWT. in International Conference on Material, Machines and Methods for Sustainable Development. 2020. Springer.

[13] Tu, T.N. and N.M. Chien, Comparison Of Different Approaches For Calculation Of Propeller Open Water Characteristic Using RANSE Method. Naval Engineers Journal, 2018. 130(1): p. 105-111.

[14] Kinaci, O.K., Straight-ahead self-propulsion and turning maneuvers of DTC container ship with direct CFD simulations. Ocean Engineering, 2022. 244: p. 110381.

[15] Kinaci, O.K., et al., On self-propulsion assessment of marine vehicles. Brodogradnja: Teorija i praksa brodogradnje i pomorske tehnike, 2018. 69(4): p. 29-51.

[16] Kinaci, O.K., et al., Free-running tests for DTC self-propulsion–An investigation of lateral forces due to the rudder and the propeller. Applied Ocean Research, 2021. 116: p. 102877.
[17] Gaggero, S., et al., Ship self-propulsion performance prediction by using OpenFOAM and different simplified propeller models, in Progress in Maritime Technology and Engineering. 2018, CRC Press. p. 195-203.
[18] Sezen, S., et al., Investigation of self-propulsion of DARPA Suboff by RANS method. Ocean Engineering, 2018. 150: p. 258-271.
[19] Sezen, S., et al., An investigation of scale effects on the self-propulsion characteristics of a submarine. Applied Ocean Research, 2021. 113: p. 102728.
[20] Sun, W., et al., Numerical Analysis of Full-Scale Ship Self-Propulsion Performance with Direct Comparison to Statistical Sea Trail Results. Journal of Marine Science and Engineering, 2020. 8(1): p. 24.
[21] Hino, T., et al., Numerical Ship Hydrodynamics: An Assessment of the Tokyo 2015 Workshop. Vol. 94. 2020: Springer Nature.
[22] https://t2015.nmri.go.jp/Instructions_JBC/instruction_JBC.html. Available from: https://t2015.nmri.go.jp/Instructions_JBC/instruction_JBC.html.
[23] ITTC 2014. Recommended Procedures and Guidelines 7.5-03-02-04. Practical Guidelines for Ship Resistance CFD. Available from: https://www.ittc.info/media/8169/75-03-03-01.pdf.
[24] Tu, T.N., et al., Effects of Turbulence Models On RANSE Computation Of Flow Around DTMB 5415 Vessel. Naval Engineers Journal, 2021. 133(3): p. 137-151.
[25] https://ittc.info/media/1587/75-02-03-011.pdf.